Upconversion processes in Er^{3+}-doped KPb_2Cl_5

R. Balda,[1,2,3] A. J. Garcia-Adeva,[1] M. Voda,[1] and J. Fernández[1,2,3]
[1]*Departamento Fisica Aplicada I, Escuela Superior de Ingenieros, Alda. Urquijo s/n, 48013 Bilbao, Spain*
[2]*Centro Mixto CSIC-UPV/EHU, Basque Country, Spain*
[3]*Donostia International Physics Center (DIPC), Basque Country, Spain*
(Received 2 December 2003; revised manuscript received 3 March 2004; published 24 May 2004)

In this work we report infrared to visible upconversion luminescence in the low phonon-energy host material KPb_2Cl_5 doped with Er^{3+} ions under $^4I_{9/2}$ excitation. The upconversion mechanisms are investigated by using steady-state and time-resolved laser spectroscopy. When the excitation wavelength is resonant with the $^4I_{9/2}$ level ($\approx$800 nm), the upconverted emission originates from the levels $^2H_{9/2}$ and $^4S_{3/2}$. These upconverted emissions occur via energy-transfer upconversion processes. However, under nonresonant excitation at lower energies than $^4I_{9/2}$, the main emission results from the level $^2H_{9/2}$. This latter upconverted emission can be attributed to excited-state absorption of the pump radiation. The proposed upconversion mechanisms responsible for the different emissions from the levels $^2H_{9/2}$ and $^4S_{3/2}$ are supported by both the time evolution of the upconversion luminescence after pulsed infrared excitation and the upconversion luminescence excitation spectra. Rate equation analysis has been used to identify and characterize the energy-transfer processes responsible for the observed fluorescence behavior.

DOI: 10.1103/PhysRevB.69.205203 PACS number(s): 78.20.−e, 78.55.Hx, 42.70.Hj, 42.65.Ky

I. INTRODUCTION

Recently, the interest in upconversion emission in rare-earth (RE) doped materials has been increased because of the search for all solid-state compact laser devices operating in the visible region and the availability of powerful near-infrared laser diodes. The potential applications include detection of infrared radiation by converting infrared signals into the visible range and upconversion lasers.[1–4] In order to investigate new upconversion materials with high luminescence efficiency, hosts with low phonon energies are required. The advantage of sulfide- and chloride-based hosts over the most extensively studied fluoride compounds is the lower phonon energy that leads to a significant reduction of the multiphonon relaxation rates. This allows an increased lifetime of some excited levels that can relax radiatively or can store energy for further upconversion, cross-relaxation, or energy-transfer processes. However, these materials usually present poor mechanical properties, moisture sensitivity, and are difficult to synthesize. Potassium lead chloride, KPb_2Cl_5, has been studied as a promising host for RE ions[5–10] because it is nonhygroscopic and readily incorporates rare-earth ions. The crystal is biaxial, crystallizes in the monoclinic system[11] (space group $P2_1/c$) with lattice parameters $a=0.8831$ nm, $b=0.7886$ nm, $c=1.243$ nm, and $\beta=90.14°$, and it is transparent in the 0.3 to 20 μm spectral region. The RE ions are supposed to substitute the lead (Pb^{2+}) ions and potassium (K^+) vacancies are assumed to provide charge compensation.[7] According to Raman-scattering measurements[7] the maximum phonon energy, measured at the highest energy peak of the spectrum, is 203 cm^{-1}. Efficient infrared to visible upconversion in this crystal when doped with Pr^{3+} ions and co-doped with Yb^{3+} ions has been recently reported by our group.[12]

In the near-infrared spectral region, Er^{3+} has a favorable energy-level structure with two transitions $^4I_{15/2}\rightarrow{}^4I_{11/2}$ (at $\approx$980 nm) and $^4I_{15/2}\rightarrow{}^4I_{9/2}$ (at $\approx$800 nm) that can be efficiently excited with high power semiconductor lasers, yielding blue, green, and red emission. In oxide and fluoride systems, excitation into the $^4I_{9/2}$ level is followed by fast nonradiative decay to the $^4I_{11/2}$ level due to the relatively high phonon energies, so this latter level acts as a long-lived intermediate state for upconversion processes. However, in chloride systems the energy gap between the $^4I_{9/2}$ and $^4I_{11/2}$ levels is too large to be effectively bridged by multiphonon relaxation and, in this case, the $^4I_{9/2}$ level acts as an intermediate level for upconversion leading to different upconversion mechanims.[13–15] In this work we analyze the upconversion processes following excitation into the $^4I_{9/2}$ level in the low phonon energy KPb_2Cl_5 crystal by using steady-state and time-resolved luminescence spectroscopy. Resonant excitation of the $^4I_{9/2}$ level leads to fluorescence from the $^2H_{9/2}$ and $^4S_{3/2}$ levels, whereas excitation at lower energies than $^4I_{9/2}$ results in emission mainly from $^2H_{9/2}$. This latter upconversion emission can be attributed to a sequential two-photon absorption. However, under resonant pumping of the $^4I_{9/2}$ level, the mechanisms to populate the $^2H_{9/2}$ and $^4S_{3/2}$ levels are energy-transfer upconversion processes. As we shall see latter, in spite of the relatively small number of energy levels involved in the upconversion processes, the mechanisms by which this upconversion takes place are numerous and there are more involved than the apparent simplicity of the experimental emission profiles seems to suggest.

II. EXPERIMENTAL TECHNIQUES

Single crystals of nonhygroscopic ternary potassium-lead chloride KPb_2Cl_5 doped with Er^{3+} ions, typically 3-cm-long and 2-cm-in diameter, have been grown in our laboratory by the Bridgman technique in a chlorine atmosphere with a two-zone transparent furnace, a vertical temperature gradient of 18 °C/cm, and a 1 mm per hour growth rate. Quartz ampoules with a tapered end were used as seed selectors to

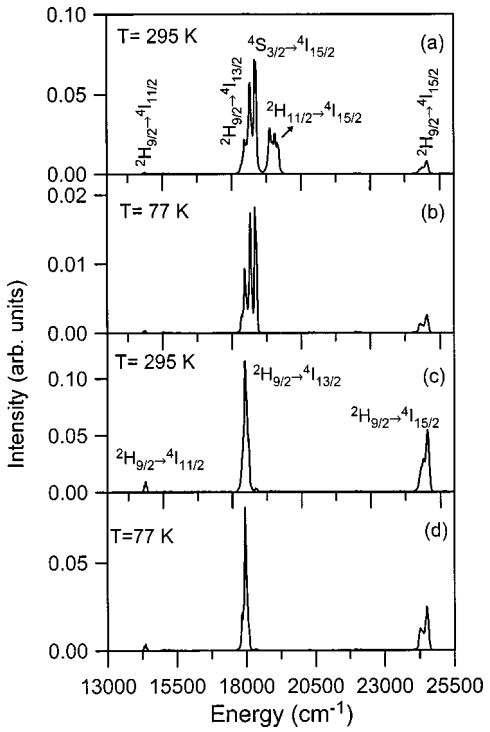

FIG. 1. Upconversion emission spectra obtained under near-infrared excitation at 12 484 cm^{-1} at 295 K (a) and 77 K (b) and under excitation at 12 180 cm^{-1} at 295 K (c) and 77 K (d).

promote single-crystal growth. The pure crystals are transparent and colorless. The Er^{3+} content did not exceed 1 mol % in the melt. Plates with approximate dimensions of $10\times6\times3$ mm^3 were cut from the blocks and adequately polished for spectroscopic measurements.

The sample temperature was varied between 4.2 and 300 K with a continuous flow cryostat. Conventional absorption spectra between 175 and 3000 nm were performed with a Cary 5 spectrophotometer. The steady-state emission measurements were made with a Ti-sapphire ring laser (0.4-cm^{-1} linewidth) as an exciting light source. The excitation beam was focused on the crystal by using a 50-mm focal lens. The fluorescence was analyzed with a 0.25-m monochromator, and the signal was detected by a Hamamatsu R928 photomultiplier and finally amplified by standard lock-in technique. Lifetime measurements were obtained by exciting the sample with a dye laser pumped by a pulsed nitrogen laser and a Ti-sapphire laser pumped by a pulsed frequency doubled Nd:YAG (yttrium aluminum garnet) laser (9-ns pulse width), and detecting the emission with Hamamatsu R928 and R5509-72 photomultipliers. The data were processed by a Tektronix oscilloscope.

III. RESULTS

Visible upconversion has been observed at room temperature under continuous wave (cw) and pulsed laser excitation in resonance with the $^4I_{9/2}$ level. The upconverted emission spectra obtained under cw excitation were measured by using a Ti-sapphire ring laser. Cut-off filters were used to remove the pump radiation. As an example Fig. 1 shows the

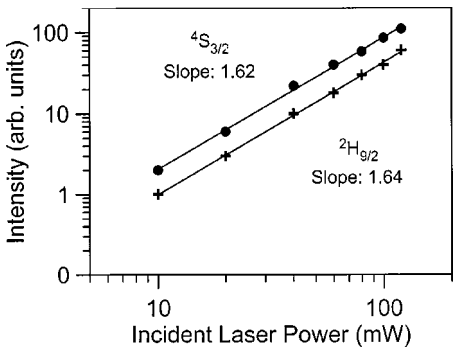

FIG. 2. Logarithmic plot of the integrated intensities of the upconverted emission from levels $^2H_{9/2}$ (24 510 cm^{-1}) and $^4S_{3/2}$ (18 349 cm^{-1}) obtained under excitation at 12 484 cm^{-1}.

upconverted emission spectra of Er^{3+}-doped KPb_2Cl_5 obtained under cw near infrared excitation at 12484 cm^{-1} in resonance with the $^4I_{15/2}\rightarrow{}^4I_{9/2}$ transition and at 12 180 cm^{-1}, and at two different temperatures, 295 and 77 K. The observed emission under excitation at 12484 cm^{-1} [Figs. 1(a) and 1(b)] corresponds to the transitions $^2H_{9/2}\rightarrow{}^4I_{15/2}$ (24510 cm^{-1}), $^2H_{11/2}\rightarrow{}^4I_{15/2}$ (18904 cm^{-1}), $^4S_{3/2}\rightarrow{}^4I_{15/2}$ (18349 cm^{-1}), $^2H_{9/2}\rightarrow{}^4I_{13/2}$ (17953 cm^{-1}), and $^2H_{9/2}\rightarrow{}^4I_{11/2}$ (14389 cm^{-1}). The $^2H_{11/2}\rightarrow{}^4I_{15/2}$ emission is only observed at room temperature because the $^2H_{11/2}$ level is populated from $^4S_{3/2}$ via a fast thermalization between both levels. As can be observed the most intense emission corresponds to the green emission from the level $^4S_{3/2}$. Under excitation at 12 180 cm^{-1}, below the $^4I_{9/2}$ level, the upconverted luminescence spectrum is mainly characterized by emissions from the level $^2H_{9/2}$. The spectra show three main bands corresponding to transitions $^2H_{9/2}\rightarrow{}^4I_{15/2,13/2,11/2}$ with no significant differences with temperature [Figs. 1(c) and 1(d)]. The emission spectrum also shows a very weak emission from the ($^2H_{11/2}$,$^4S_{3/2}$) levels at room temperature. The $^2H_{11/2}$ emission disappears at 77 K.

To investigate the excitation mechanisms for populating the $^2H_{9/2}$ and $^4S_{3/2}$ levels after IR excitation, we have obtained the IR emission intensities for different pumping powers. The upconversion emission intensity (I_{em}) depends on the incident pump power (P_{pump}) according to the relation $I_{em}\propto(P_{pump})^n$, where n is the number of photons involved in the pumping process. The upconversion intensities were recorded at 24 510 cm^{-1} ($^2H_{9/2}$) and 18 349 cm^{-1} ($^4S_{3/2}$) for different pump powers. Figure 2 shows a logarithmic plot of the integrated emission intensity of the upconverted fluorescence as a function of the pump laser intensity. The dependence of the intensity on the pump power is close to quadratic, which indicates a two-photon (TP) upconversion process to populate the $^2H_{9/2}$ and $^4S_{3/2}$ levels.

To further investigate the nature of the upconversion processes, excitation spectra of the emissions at 24 510 cm^{-1} ($^2H_{9/2}$) and 18349 cm^{-1} ($^4S_{3/2}$) were performed between 77 and 295 K in the spectral region corresponding to the $^4I_{15/2}\rightarrow{}^4I_{9/2}$ transition. The excitation spectra were corrected for the spectral variation of the laser intensity. Figure 3 shows for comparison the room-temperature excitation spectra for the upconverted emissions by monitoring the $^2H_{9/2}\rightarrow{}^4I_{15/2}$

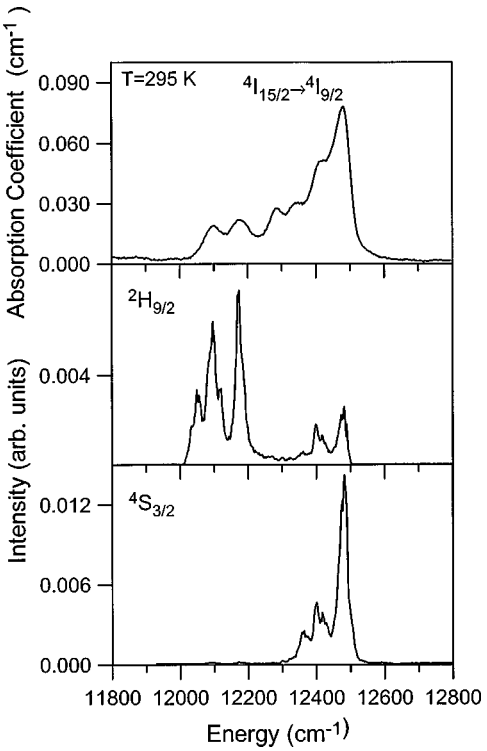

FIG. 3. Excitation spectra of the upconverted emission from levels $^2H_{9/2}$ (24 510 cm^{-1}) and $^4S_{3/2}$ (18 349 cm^{-1}), corrected for the spectral variation of the laser intensity. The one-photon absorption spectrum corresponding to $^4I_{15/2}\rightarrow{}^4I_{9/2}$ is also included for comparison.

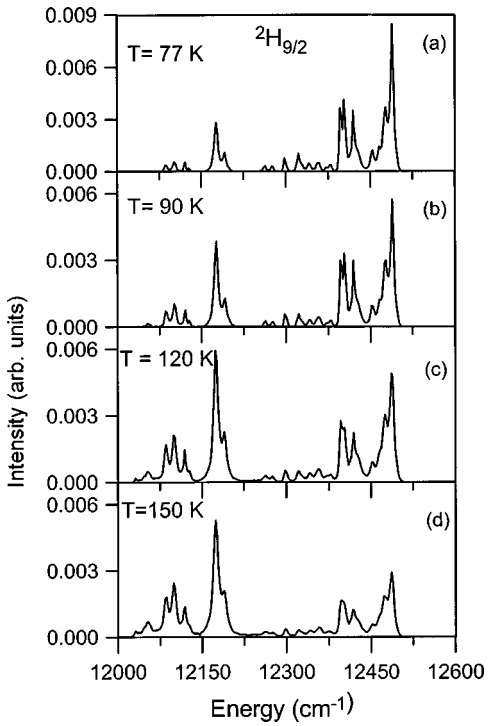

FIG. 4. Excitation spectra of the upconverted emission from level $^2H_{9/2}$ (24 510 cm^{-1}) obtained at different temperatures, corrected for the spectral variation of the laser intensity.

transition at 24 510 cm^{-1} and the $^4S_{3/2}\rightarrow{}^4I_{15/2}$ transition at 18 349 cm^{-1} together with the one-photon (OP) absorption spectrum. The excitation spectrum corresponding to the green emission from the $^4S_{3/2}$ level is very similar to the absorption spectrum whereas the excitation spectrum of the blue emission from the $^2H_{9/2}$ level resembles the absorption spectrum in the high-energy region but presents some additional peaks not observed in the OP absorption spectrum. Figure 4 shows the excitation spectrum of the blue-upconverted emission from level $^2H_{9/2}$ obtained at different temperatures. The two groups of peaks observed in the excitation spectrum show a different temperature dependence. At low temperature, the peaks at lower energies than the $^4I_{15/2}\rightarrow{}^4I_{9/2}$ transition decrease in intensity, indicating a thermally activated process.

The temporal evolution of the upconverted emissions and the infrared emission of the $^4I_{9/2}\rightarrow{}^4I_{15/2}$ transition were performed by exciting the samples in resonance with the $^4I_{9/2}$ level and nonresonantly at 12 180 cm^{-1} with a Ti-sapphire laser pumped by a frequency-doubled pulsed Nd-YAG laser. The decays and lifetimes of the $^2H_{9/2}$ and $^4S_{3/2}$ levels were also obtained under direct excitation with a dye laser. Figure 5 shows the time evolution of the upconverted $^2H_{9/2}$ emission at room temperature for two different excitation energies obtained after an infrared excitation pulse of 9 ns. The insets show the same decays but in a semilogarithmic plot. The decay obtained under excitation at 12 484 cm^{-1} in resonance with the $^4I_{15/2}\rightarrow{}^4I_{9/2}$ absorption shows a rise and a decay with a lifetime much longer than that of the $^2H_{9/2}$ level under OP excitation, whereas the decay obtained by exciting at 12 180 cm^{-1} in the additional peaks of the excitation spectrum is a single exponential with a lifetime similar to the one obtained under OP direct excitation of the $^2H_{9/2}$ level (120 μs). Figure 6 shows the experimental decays of the green emission from the level $^4S_{3/2}$ at room temperature by exciting at 19 121 cm^{-1} (523 nm) and 12484 cm^{-1} (801 nm). As can be seen, the decay curve of the upconverted emission shows a lifetime much longer than that of the level $^4S_{3/2}$ under direct excitation (238 μs).

IV. DISCUSSION

As we have seen in the previous section, the two excited levels $^2H_{9/2}$ and $^4S_{3/2}$ are responsible for the upconverted luminescence under resonant excitation into the $^4I_{9/2}$ level, whereas the main contribution to the visible luminescence under excitation at lower energies than $^4I_{9/2}$ originates from the level $^2H_{9/2}$. The pumping power dependence of the upconverted emissions from these levels indicates that a two-photon upconversion process is responsible for the emissions from the $^2H_{9/2}$ and $^4S_{3/2}$ levels. This process may be associated with excited-state absorption (ESA) involving single ions and/or energy-transfer upconversion (ETU) involving two excited ions.[16,17] It is well established that the upconversion luminescence excitation spectra and the temporal evolution of the upconversion luminescence after pulsed excitation allow us to distinguish between ESA and ETU processes.[18] In the ETU case, the excitation spectrum is proportional to the square of the OP absorption coefficient as a

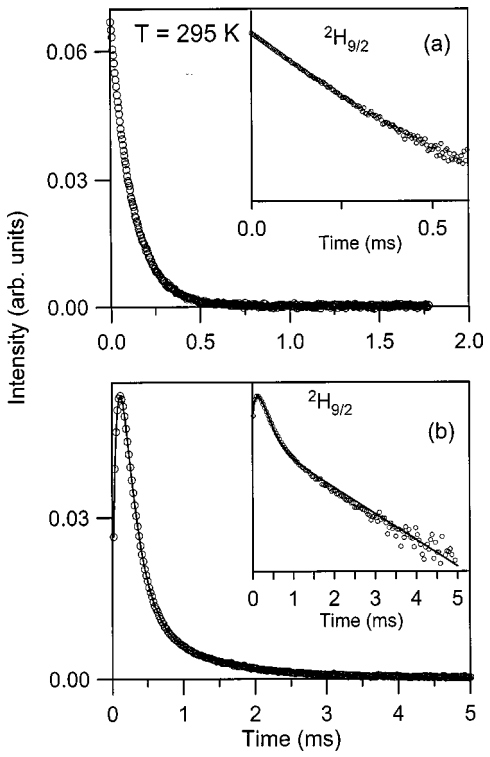

FIG. 5. Temporal behavior of the blue upconversion luminescence from the level $^2H_{9/2}$ obtained at two different excitation energies (a) 12 180 cm^{-1} and (b) 12 484 cm^{-1} (open circles) and the fit to Eq. (3a) (solid line). The inset shows the same curves in semilogarithmic representation.

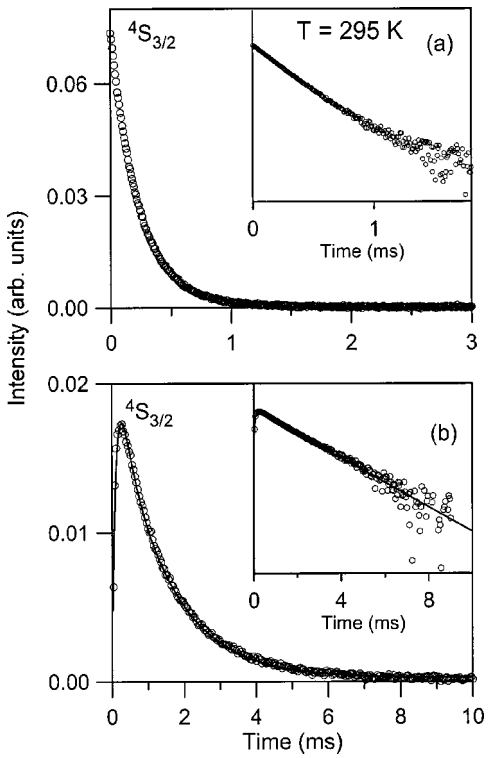

FIG. 6. Temporal behavior of the green upconversion luminescence from the level $^4S_{3/2}$ obtained at two different excitation energies (a) 19 120 cm^{-1} and (b) 12 484 cm^{-1} (open circles) and the fit to Eq. (3b) (solid line). The inset shows the same curves in semilogarithmic representation.

function of wavelength, whereas in the case of excited-state absorption the upconversion excitation spectrum is the result of OP absorption and excited-state absorption.

In the present system, the $^4I_{9/2}$ state acts as a sensitizer for both Er^{3+} ions and therefore an excitation spectrum similar to the OP absorption spectrum is expected for the ETU process. Indeed, the high-energy side of the excitation spectrum of the upconverted luminescence from the level $^2H_{9/2}$ shows the presence of peaks corresponding to the $^4I_{15/2}\rightarrow{}^4I_{9/2}$ absorption of the Er^{3+} ions (Figs. 3 and 4). This indicates that an ETU process from the $^4I_{9/2}$ multiplet takes place. However, the spectrum also presents additional intense peaks at energies that are resonant with the $^4I_{9/2}\rightarrow{}^2H_{9/2}$ transition. This indicates that ESA is the dominant mechanism for the $^2H_{9/2}$ emission obtained under nonresonant excitation at lower energies than the $^4I_{15/2}\rightarrow{}^4I_{9/2}$ transition, and it can be explained by the pumping mechanism described in Fig. 7. In a first step, the absorption of one IR pump-photon excites the ions to the $^4I_{9/2}$ level and a subsequent ESA of a second pump photon promotes the ions to the $^2H_{9/2}$ level. In this process the first step $^4I_{15/2}\rightarrow{}^4I_{9/2}$ needs to be thermally activated because the excitation energy is 300 cm^{-1} lower than the $^4I_{15/2}\rightarrow{}^4I_{9/2}$ transition at low temperatures. The thermal activation can be achieved at room temperature by absorption from higher crystal-field levels of the ground state as can be seen in the absorption spectrum in Fig. 3. As a consequence this ESA process is less efficient at low temperature as we have seen in Fig. 4. In conclusion, as shown in the energy-level diagram of Fig. 7, both ESA and ETU processes contribute to the upconversion luminescence from the $^2H_{9/2}$ level depending on the excitation energy. These results are further confirmed by the time evolution of the upconverted luminescence.

The excitation spectrum of the upconverted green emission from the level $^4S_{3/2}$ follows the same wavelength de-

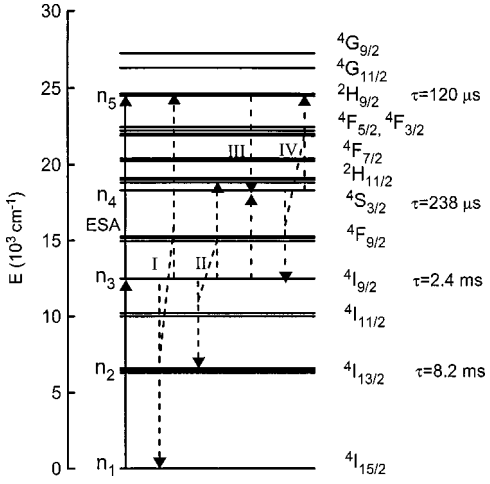

FIG. 7. Energy-level diagram of Er^{3+} in KPb_2Cl_5 and the possible upconversion mechanisms to populate the $^2H_{9/2}$ and $^4S_{3/2}$ levels. The dashed lines refer to ETU processes after resonant excitation in the $^4I_{9/2}$ level.

pendence as the OP absorption spectrum. This fact clearly indicates that we are dealing with an energy-transfer upconversion (ETU) to populate the $^4S_{3/2}$ state. The population of the $^4S_{3/2}$ level through the $^2H_{9/2}$ level as an intermediate state by multiphonon relaxation can be disregarded because of the energy gap between these two levels and the phonon energies involved. From the energy levels of Er^{3+} in this crystal, one possible energy-transfer upconversion process to populate the $^4S_{3/2}$ level is $(^4I_{9/2},{}^4I_{9/2})\rightarrow(^4I_{13/2},{}^4S_{3/2})$ (Fig. 7). In this process, when two Er^{3+} ions are excited by an IR photon directly to the $^4I_{9/2}$ state, a transfer occurs by which one ion loses energy and goes to the $^4I_{13/2}$ state while the other one gains energy and goes to the $^4S_{3/2}$ state. This process is nearly resonant with an energy mismatch of 14 cm^{-1}.

The time evolution of the upconversion luminescence after an excitation pulse provides a useful tool in discerning which is the operative mechanism. The radiative ESA process occurs during the excitation pulse and leads to an immediate decay of the upconversion luminescence after excitation. Upconversion by energy transfer leads to a time-dependent emission that shows a rise time after the laser pulse followed by a decay with a lifetime longer than the one after direct excitation. This distinction is possible when the pulse width is much shorter than the time constant of the relevant energy transfer step.[18] The time evolution of the blue emission from the level $^2H_{9/2}$ obtained after an infrared excitation pulse of 9 ns shows a different behavior, depending on the excitation energy. As shown in Fig. 5(a), after nonresonant pulsed infrared excitation the resulting $^2H_{9/2}\rightarrow{}^4I_{15/2}$ upconversion luminescence intensity decays instantaneously after the laser pulse with a lifetime similar to that of the $^2H_{9/2}$ level under direct excitation (120 μs). Therefore, we conclude that the infrared to visible upconversion mechanism is the ESA process displayed in Fig. 7. For resonant excitation into the $^4I_{9/2}$ state (12 484 cm^{-1}), however, the decay curve of the upconverted fluorescence shows a rise time and a double exponential decay [Fig. 5(b)]. The two components of the decay can be seen very clearly in the semilogarithmic plot. The fast component has a lifetime of 128 μs and the lifetime of the long component is about half the lifetime of the $^4I_{9/2}$ level which is 2.4 ms. This indicates that the upconversion emission from the level $^2H_{9/2}$ is not only caused by the interaction between two Er^{3+} ions in the $^4I_{9/2}$ level (ETU). If this level were solely populated by the ETU process I shown in Fig. 7 in which two Er^{3+} ions in the $^4I_{9/2}$ level interact, the temporal behavior of the blue emission from the level $^2H_{9/2}$ would consist of a rise and a decay determined by the lifetimes of the levels involved and the energy-transfer rate constant. However, such a model can neither account for the double exponential decay nor for the fast rise time of the population of this level.

The time evolution of the emission from the $^4S_{3/2}$ level obtained after an infrared excitation pulse of 9 ns in resonance with the $^4I_{15/2}\rightarrow{}^4I_{9/2}$ transition shows a rise time of 120 μs and a decay much longer than that of level $^4S_{3/2}$ under OP excitation [see Fig. 6(b)]. The lifetime of the decay is again about half the lifetime of the $^4I_{9/2}$ level (2.4 ms) which indicates that the upconversion emission from the level $^4S_{3/2}$ is caused by interaction between two Er^{3+} ions in the $^4I_{9/2}$ level (ETU) and not by excited-state absorption. However, the observed rise time ($\sim$120 μs) cannot be described by such an ETU process. Indeed, if the ETU process would be the only one active in this system, the short-time behavior of this emission would consist of a rise [see Eq. (3b)] occurring in a time equal to the lifetime of the $^4S_{3/2}$ level ($\sim$238 μs) in contradiction with the observed behavior. Therefore, everything seems to suggest that additional processes are necessary in order to explain the time dependence of the upconverted luminescence from both the $^2H_{9/2}$ and $^4S_{3/2}$ levels.

A first clue towards identifying these additional mechanisms comes from noticing that the rise time of the population of the level $^4S_{3/2}$ is very similar to the lifetime of the level $^2H_{9/2}$ obtained under OP excitation. This kind of behavior can easily be explained by the presence of cross relaxation in which one ion in the $^2H_{9/2}$ level decays to the $^4S_{3/2}$ level and another ion in a lower level is promoted to an upper one separated by a similar energy. If the lifetime of one of the levels involved is much longer than the other one, the resulting characteristic time of the process will be very similar to the lifetime of the fastest one (see below). In fact, there are two possible processes in this system $(^2H_{9/2},{}^4I_{9/2})\rightarrow(2\ {}^4S_{3/2})$ and $(^2H_{9/2},{}^4I_{13/2})\rightarrow(^4S_{3/2},{}^4I_{9/2})$ that meet these conditions and are energetically favorable at room temperature. Besides, the lifetimes of the $^4I_{9/2}$ and $^4I_{13/2}$ levels involved are much longer than the one of $^2H_{9/2}$. However, at the early stages of the population dynamics, the population of the $^4I_{9/2}$ level is much larger than the one of $^4I_{13/2}$. Therefore, it seems reasonable to assume that the former cross-relaxation is more likely than the latter one. In fact, this cross-relaxation process has been identified as a contribution to the $^4S_{3/2}$ population in other systems,[19] too.

With regard to understanding the rise and initial decay of the population of the level $^2H_{9/2}$, it is worth noticing that the characteristic time of both the rise and the first step of the decay are very similar to the lifetime of this level and/or to half the lifetime of $^4S_{3/2}$. The simplest process one can devise in order to reproduce this behavior is another ETU process that can be cast in the form $(2\ {}^4S_{3/2})\rightarrow(^2H_{9/2},{}^4I_{9/2})$. Even though it could seem at a first glance that this process would exactly cancel the cross-relaxation described above, this is not really the case. Indeed, as we will show below in more detail, this process includes both a rise in population of the $^2H_{9/2}$ level with a characteristic time equal to the lifetime of this level plus a first step decay with a characteristic decay time equal to half the lifetime of the level $^4S_{3/2}$. Due to the fact that the prefactors of each of these terms are quite different from each other (in absolute value, see below) and that the characteristic rates of these two steps (i.e., the lifetime of $^2H_{9/2}$ is not exactly equal to half the lifetime of level $^4S_{3/2}$) are not strictly the same, such a cancellation does not really occur.

The scarce knowledge about the distribution of dopant ions in a KPb_2Cl_5 crystal makes it difficult to justify the use of macroscopic rate equations to investigate the upconversion decays. However, the lifetime measurements of the $^4I_{9/2}$ level as a function of concentration, under one-photon excitation, show the existence of fast energy migration among

donors[20] (the experimental decays remain single exponential and their inverse depend linearly on concentration), which would allow us to consider the decay of the whole ensemble of excited ions as corresponding to a collective macroscopic decay. As we shall see below, the upconversion mechanisms under pulsed excitation can be consistently modeled by means of a simple rate equation analysis. In the following, we will use the notation n_1, n_2, n_3, n_4, and n_5 to represent the populations of levels $^4I_{15/2}$, $^4I_{13/2}$, $^4I_{9/2}$, $^4S_{3/2}$, and $^2H_{9/2}$, respectively. The rate equations that include all the possible ETU mechanisms for infrared upconversion described above are given by

$$\dot{n}_1(t) = \frac{n_2}{\tau_2} + \frac{n_3}{\tau_3} + \frac{n_4}{\tau_4} + \frac{n_5}{\tau_5} + \gamma_I n_3^2, \tag{1a}$$

$$\dot{n}_2(t) = -\frac{n_2}{\tau_2} + \gamma_{II} n_3^2, \tag{1b}$$

$$\dot{n}_3(t) = -\frac{n_3}{\tau_3} - 2\gamma_I n_3^2 - 2\gamma_{II} n_3^2 - \gamma_{III} n_3 n_5 + \gamma_{IV} n_4^2, \tag{1c}$$

$$\dot{n}_4(t) = -\frac{n_4}{\tau_4} + \gamma_{II} n_3^2 + 2\gamma_{III} n_3 n_5 - 2\gamma_{IV} n_4^2, \tag{1d}$$

$$\dot{n}_5(t) = -\frac{n_5}{\tau_5} + \gamma_I n_3^2 - \gamma_{III} n_3 n_5 + \gamma_{IV} n_4^2. \tag{1e}$$

In these expressions, γ_I, γ_{II}, γ_{III}, and γ_{IV} are the coefficients of the ETU mechanisms depicted in Fig. 7 and described above and τ_i are the experimental lifetimes obtained under OP excitation. In writing down Eqs. (1), some approximations are involved. First of all, the terms describing the ESA processes are not included. The reason is that these processes occur on a time scale much shorter (pulse duration) than the time scale of the $^2H_{9/2}$ and $^4S_{3/2}$ decays. This implies that by the time the first data points are acquired, the ESA processes have already taken place. Therefore, the effect of these processes on the time scale of interest (ms) can be substituted to an excellent approximation by initial populations of the levels involved. We have also neglected the population of the $^4I_{11/2}$ and $^4I_{13/2}$ states by radiative transitions from levels $^2H_{9/2}$ and $^4S_{3/2}$ since states $^4I_{11/2}$ and $^4I_{13/2}$ do not lead to a situation from which a further ETU process can take place, and therefore have no influence over the population of levels $^2H_{9/2}$ and $^4S_{3/2}$.

It is easy to realize that the coupled system (1) does not admit a closed solution in terms of elementary functions. However, it is easy to find analytical approximations to this solution under some reasonable approximations. In particular, assuming that

$$\frac{n_3}{\tau_3} \gg 2\gamma_I n_3^2 + 2\gamma_{II} n_3^2 + \gamma_{III} n_3 n_5 - \gamma_{IV} n_4^2, \tag{2}$$

i.e., the radiative component is much larger than any other term that depopulates $^4I_{9/2}$, the rate equations (1) can be solved to leading order in the ETU coefficients. This approximation is usually well justified and, in our particular case, it is experimentally observed that n_3 follows an exponential decay with a rate constant similar to τ_3, which implies that Eq. (2) constitutes a very good approximation. Under this condition, Eqs. (1d) and (1e) can be solved perturbatively to first order in the ETU coefficients. The resulting time evolution of the decays is given by

$$n_5(t) = n'_{50} e^{-t/\tau_5} + \gamma'_I e^{-2t/\tau_3} + \gamma'_{IV} e^{-2t/\tau_4}, \tag{3a}$$

$$n_4(t) = n'_{40} e^{-t/\tau_4} + \gamma'_{II} e^{-2t/\tau_3} + \gamma'_{III} e^{-t/\tau_5}. \tag{3b}$$

Thereby we have introduced the notations $n'_{50} = n_{50} - \gamma'_I - \gamma'_{IV}$, $n'_{40} = n_{40} - \gamma'_{II} - \gamma'_{III}$ and the following abbreviations:

$$\gamma'_I = \gamma_I n_{30}^2 \frac{\tau_3 \tau_5}{\tau_3 - 2\tau_5}, \tag{4a}$$

$$\gamma'_{II} = \gamma_{II} n_{30}^2 \frac{\tau_3 \tau_4}{\tau_3 - 2\tau_4}, \tag{4b}$$

$$\gamma'_{III} = 2\gamma_{III} n_{30} n_{50} \frac{\tau_4 \tau_5}{\tau_5 - \tau_4}, \tag{4c}$$

$$\gamma'_{IV} = \gamma_{IV} n_{40}^2 \frac{\tau_4 \tau_5}{\tau_4 - 2\tau_5}. \tag{4d}$$

Apart from the perturbative approach which leads to Eqs. (3), three other approximations worth noticing have been used. The first one consists of taking $(1/\tau_5) + (1/\tau_3) \approx 1/\tau_5$, which is well justified by the fact that the lifetime of the level $^4I_{9/2}$ is ten times longer than the one of $^2H_{9/2}$. The second one consists of neglecting a γ'_{III} term in n'_{50}. From Eqs. (4c) and (4d), it is obvious that this approximation is also well justified as $\gamma'_{III} \ll \gamma'_{IV}$. Finally, the term $\gamma'_{III} e^{-2t/\tau_4}$ has been neglected in Eq. (3a) for the same reason as before.

There are some features of Eqs. (3) that are worth mentioning. First of all, due to the fact that $\tau_4 \approx 2\tau_5$ (but $\tau_4 < 2\tau_5$), γ'_{IV} will be very large compared to the other γ', and negative. Also, under resonant pumping of the level $^4I_{9/2}$, an ESA mechanism that populates $^2H_{9/2}$ will be very inefficient and n_{50} will be very small. This means that in Eq. (3a), the term proportional to γ'_{IV} dominates the emission dynamics at short times ($t < \tau_3/2$), even for a modest initial population of the $^2H_{9/2}$ level. Therefore, Eq. (3a) describes a rise in the population of the $^2H_{9/2}$ level with a characteristic time given by τ_5 and a two-step decay for $t > \tau_5$. The first step ($t < \tau_3/2$) exhibits a characteristic decay time of $\tau_4/2$ and the second step ($t > \tau_3/2$) exhibits a characteristic decay time of $\tau_3/2$. This behavior is in qualitative agreement with the observed data. It is also important to stress that, were the terms proportional to γ'_{IV} absent, the predicted behavior would be a two-step decay with characteristic times τ_5 and $\tau_3/2$ or, for a very inefficient ESA process, only the $\tau_3/2$ component would appear. Equation (3b), on the other hand, describes a rise of the population of the $^4S_{3/2}$ level with a characteristic rise time given by τ_5 (which is due to the fact that n_{40} is even smaller than n_{50}, as there are no direct processes which populate the $^4S_{3/2}$ level and because γ'_{III} is negative) and a

subsequent decay characterized by $\tau_3/2$, also in qualitative agreement with the observed behavior.

Once we have justified that these ETU processes can qualitatively describe the population dynamics of the $^2H_{9/2}$ and $^4S_{3/2}$ levels under pulsed excitation, we can fit the experimental data to the analytical approximations provided by Eqs. (3). The resulting fits are reported in Figs. 5 and 6 for the blue and green emissions, respectively. The values for the ETU coefficients obtained from those fits are 4470, 5800, 2433, and 3368 s^{-1} for γ_{I}, γ_{II}, γ_{III}, and γ_{IV}, respectively. It is worth noticing that the theoretical curves are in excellent agreement with the experimental ones in the whole temporal range and for both emissions, which is a strong support for the validity of the model described above.

V. CONCLUSIONS

IR-to-visible upconversion in the Er^{3+}-doped low phonon-energy crystal KPb_2Cl_5 has been investigated under continuous wave and pulsed laser excitation into the $^4I_{9/2}$ level. Resonant excitation of level $^4I_{9/2}$ leads to emission from levels $^2H_{9/2}$ and $^4S_{3/2}$, whereas nonresonant excitation at lower energies than $^4I_{9/2}$ resuls in emission mainly from the level $^2H_{9/2}$. The analysis of the experimental results as a function of excitation wavelength and time confirms the existence of two different upconversion mechanisms (ESA and ETU) to populate level $^2H_{9/2}$, depending on the excitation energy. Under nonresonant pulsed excitation the time evolution of the upconverted emission from the level $^2H_{9/2}$ shows an immediate decay with the same lifetime as the one obtained after direct excitation, which indicates an ESA process is populating this level. Resonant pulsed excitation of the level $^4I_{9/2}$ leads to fluorescence having a rise and a double exponential decay. The lifetime of the long decay component is about half the lifetime of the level $^4I_{9/2}$ which indicates an ETU process involving two Er^{3+} ions in this level. The excitation wavelength dependence of the green emission from the level $^4S_{3/2}$ together with the time evolution of the decays suggest that an ETU process involving two Er^{3+} ions in the $^4I_{9/2}$ level is responsible for this emission. However, these two ETU mechanisms cannot explain the temporal behavior of the upconverted emissions from levels $^2H_{9/2}$ and $^4S_{3/2}$. The inclusion of two additional two-ion processes was found to be necessary in order to explain the experimental fluorescence decays. The temporal dynamics of the upconverted emissions under pulsed excitation has been modeled by a simple rate equation analysis. This model is found to describe very well the temporal dynamics of both the blue and green emissions in the whole temporal range. It is also important to stress that by an adequate tuning of the excitation wavelength we are able to select the upconversion emitting level and the upconversion mechanism.

ACKNOWLEDGMENTS

This work was supported by the Spanish Government MCYT (Contract Nos. BFM2000-0352 and MAT2000-1135), Basque Country Government (Contract No. PI-1999-95), and Basque Country University (Grant No. UPV13525/2001). One of us (A.J.G.-A.) wants to thank the Spanish MCYT for financial support under the ''Ramón y Cajal'' program.

APPENDIX: PERTURBATIVE ANALYSIS OF THE RATE EQUATION MODEL

Let us briefly outline how the solution of the rate equations (1) to first order in the ETU coefficients proceeds. If approximation (2) holds, Eq. (1c) immediately reads

$$\dot{n}_3(t) = -\frac{n_3}{\tau_3}, \tag{A1}$$

which admits the trivial solution

$$n_3(t) = n_{30} e^{-t/\tau_3}, \tag{A2}$$

with n_{30} the initial population of level $^4I_{9/2}$. To solve the corresponding equation for $n_4(t)$ we assume without loss of generality that this function can be cast as

$$n_4(t) = n_{40} e^{-t/\tau_4} + n_4^{(1)}(t;\gamma_i), \tag{A3}$$

where the second summand on the right member contains all the dependence on the ETU coefficients. By inserting (A3) into (1d) and keeping only terms linear in the ETU coefficients, we arrive at

$$\dot{n}_4^{(1)}(t) \approx -\frac{n_4^{(1)}}{\tau_4} + \gamma_{\mathrm{II}} n_{30}^2 e^{-2t/\tau_3} + 2\gamma_{\mathrm{III}} n_{30} n_{50} e^{-t(1/\tau_3 + 1/\tau_5)} - 2\gamma_{\mathrm{IV}} n_{40}^2 e^{-2t/\tau_4}. \tag{A4}$$

This equation can be trivially solved to give

$$n_4^{(1)}(t) \approx C e^{-t/\tau_4} + \gamma'_{\mathrm{II}} e^{-2t/\tau_3} + 2\gamma_{\mathrm{III}} n_{30} n_{50} \times \left(\frac{1}{\tau_4} - \frac{1}{\tau_3} - \frac{1}{\tau_5}\right)^{-1} e^{-t(1/\tau_3 + 1/\tau_5)} + 2\gamma_{\mathrm{IV}} n_{40}^2 \tau_4 e^{-2t/\tau_4}, \tag{A5}$$

where

$$C = -\gamma'_{\mathrm{II}} - 2\gamma_{\mathrm{III}} n_{30} n_{50} \left(\frac{1}{\tau_4} - \frac{1}{\tau_3} - \frac{1}{\tau_5}\right)^{-1} + 2\gamma_{\mathrm{IV}} n_{40}^2 \tau_4. \tag{A6}$$

Taking into account that $n_{40} \ll n_{30}$, the term proportional to γ_{IV} can be dropped. Making use of the fact $\tau_3 \gg \tau_4$, τ_5 we finally arrive to Eq. (3b). The derivation of Eq. (3a) proceeds along the same lines, so it will not be presented here.

[1] G.L. Vossler, C.L. Brooks, and K.A. Winik, Electron. Lett. **31**, 1162 (1995).
[2] T.H. Whitley, C.A. Millar, R. Wyatt, M.C. Brierley, and D. Szebesta, Electron. Lett. **27**, 1785 (1991).
[3] J.E. Roman, P. Camy, M. Hempstead, W.S. Brocklesby, S. Nouth, A. Beguin, C. Lerminiaux, and J.S. Wilkinson, Electron. Lett. **31**, 1345 (1995).
[4] A. Pollack and D.B. Chang, J. Appl. Phys. **64**, 2885 (1988).
[5] M.C. Nostrand, R.H. Page, S.A. Payne, W.F. Krupke, P.G. Schunemann, and L.I. Isaenko, OSA Trends Opt. Photonics Ser. **19**, 524 (1998).
[6] M.C. Nostrand, R.H. Page, S.A. Payne, W.F. Krupke, P.G. Schunemann, and L.I. Isaenko, OSA Trends Opt. Photonics Ser. **26**, 441 (1999).
[7] M.C. Nostrand, R.H. Page, S.A. Payne, L.I. Isaenko, and A.P. Yelisseyev, J. Opt. Soc. Am. B **18**, 264 (2001).
[8] R. Balda, M. Voda, M. Al-Saleh, and J. Fernández, J. Lumin. **97**, 94 (2002).
[9] A. Mendioroz, J. Fernández, M. Voda, M. Al-Saleh, A.J. Garcia-Adeva, and R. Balda, Opt. Lett. **27**, 1525 (2002).
[10] N.W. Jenkins, S.R. Bowman, S. O'Connor, S.K. Searles, and J. Ganem, Opt. Mater. (Amsterdam, Neth.) **22**, 311 (2003).
[11] K. Nitsch, M. Dusek, M. Nikl, K. Polák, and M. Rodová, Prog. Cryst. Growth Charact. Mater. **30**, 1 (1995).
[12] R. Balda, J. Fernández, A. Mendioroz, M. Voda, and M. Al-Saleh, Phys. Rev. B **68**, 165101 (2003).
[13] M.P. Hehlen, K. Krämer, H.U. Güdel, R.A. McFarlane, and R.N. Schwartz, Phys. Rev. B **49**, 12 475 (1994).
[14] T. Riedener, P. Egger, J. Hulliger, and H.U. Güdel, Phys. Rev. B **56**, 1800 (1997).
[15] S.R. Lüthi, M. Pollnau, H.U. Güdel, and M.P. Hehlen, Phys. Rev. B **60**, 162 (1999).
[16] F. Auzel, Proc. IEEE **61**, 758 (1973).
[17] J.C. Wright, Top. Appl. Phys. **15**, 239 (1976).
[18] T. Riedener and H.U. Güdel, J. Chem. Phys. **107**, 2169 (1997).
[19] M.P. Hehlen, G. Frei, and H.U. Güdel, Phys. Rev. B **50**, 16 264 (1994).
[20] M.J. Weber, Phys. Rev. B **4**, 2932 (1971).